AAS 13-805

PRELIMINARY ANALYSIS OF BALLISTIC TRAJECTORIES TO NEPTUNE VIA GRAVITY ASSISTS FROM VENUS, EARTH, MARS, JUPITER, SATURN, AND URANUS

Kyle M. Hughes*, James W. Moore†, and James M. Longuski‡

Ballistic gravity-assist trajectories to Neptune are investigated with Earth launch dates ranging from the years 2020 to 2070. One impulsive maneuver is allowed, with up to 3 km/s ΔV, for trajectories that are unable to reach Neptune ballistically. Trajectories are identified using patched-conic techniques with an analytic ephemeris. Classical flyby sequences (e.g. Venus-Earth-Earth-Jupiter), as well as less conventional sequences (that may include flybys of Saturn or Uranus), are considered and compared. Trajectories are constrained to flight times of 15 years or less, and desirable trajectories with regard to parameters such as time of flight, launch date, launch V_∞, arrival V_∞, and ΔV cost are selected and discussed. Of the 76 paths investigated, 21 were found to produce trajectories that satisfied the constraints of this study. The more desirable of these trajectories include a flyby of Jupiter; however, for launch dates when Jupiter is unavailable (such as around 2022 to 2030), direct launch to Neptune or a flyby of Saturn can be used at the cost of a larger ΔV at launch.

INTRODUCTION

Recent mission concept studies for the 2010 decadal survey have indicated much interest in the last two outer planets—Uranus and Neptune.[1,2] For the case of Neptune, missions for both flyby of and capture into the Neptune system are proposed—including studies of Neptune's largest moon Triton. Some of these proposed missions go beyond the Neptune system to investigate Kuiper Belt Objects (KBOs). Trajectories to Neptune typically require high launch energies, long times of flight (TOF), and high arrival energies. As a result, nearly all proposed trajectories to Neptune involve a Jupiter gravity assist (JGA), which in turn restricts most Neptune-bound missions to take place during periods of time when Jupiter is available.

Broad searches for trajectory opportunities to the outer planets have been studied in previous years. In 1991, Longuski and Williams[3] investigated ballistic trajectories to Pluto, and discovered a four-planet grand tour opportunity in 1996, with flybys of Jupiter, Uranus, Neptune and Pluto. Ballistic trajectories to Pluto were also investigated by Sims et al.[4] in 1997, for the Pluto Express mission. These trajectories were constrained to arrive at Pluto within 12 years, and contain no flybys of Earth. To obtain such trajectories, Sims et al. allowed for the implementation of impulsive deep-space maneuvers. All of the trajectories found by Sims et al. included JGAs, and some allowed for flybys of asteroids such as Seraphina.

In 2000, Petropoulos et al.[5] investigated ballistic trajectories to Jupiter over a large span of launch dates ranging from 1999 to 2030. In their paper, 'classical' sequences of flyby bodies (or 'paths') were found, such as of Venus and Earth, respectively, as well as nonconventional paths, such as Venus-Mars-Venus-Earth. In 2011, Spreen et al.[6] conducted a similar investigation (to that of Petropoulos et al.) for ballistic trajectories to Uranus for Earth launch dates ranging from the years 2020 to 2060.

*Doctoral Candidate, School of Aeronautics and Astronautics, Purdue University, 701 W. Stadium Ave., West Lafayette, IN 47907-2045, kylehughes@purdue.edu, AIAA Student Member.

†Doctoral Candidate, School of Aeronautics and Astronautics, Purdue University, 701 W. Stadium Ave., West Lafayette, IN 47907-2045, moore38@purdue.edu, AIAA Member.

‡Professor, School of Aeronautics and Astronautics, Purdue University, 701 W. Stadium Ave., West Lafayette, IN 47907-2045, longuski@purdue.edu, AAS Member, AIAA Associate Fellow.

In all of these previously mentioned studies, the broad search of trajectories was done using a patched-conic propagator with analytic ephemeris. Optimization techniques, however, have also been applied to ballistic gravity-assist trajectories, such as by Melman et al.,[7] who implemented genetic algorithms to find an optimal trajectory to Neptune, as well as an optimal tour of the Neptune system.

Broad searches for low-thrust opportunities to the outer planets have also been investigated, such as by Landau et al.,[8] who found a variety of solar electric propulsion (SEP) low-thrust trajectories, with launch dates spanning from 2015 to 2035. The SEP trajectories were found using the low-thrust optimization tool MALTO[9] developed at the Jet Propulsion Laboratory (JPL). Other methods for the design of optimal low-thrust gravity-assist trajectories have been proposed, such as by Casalino et al.,[10] who focused on low-thrust trajectories to escape the Solar System, and Zimmer and Ocampo,[11] who applied analytical gradients to optimize low-thrust trajectories. More recently, Yam et al.[12] used global optimization techniques for low-thrust gravity-assist trajectories to Jupiter.

METHODOLOGY

The basic methodology for this study is as follows.

First, a list of gravity-assist paths will be generated to account for all combinations of flyby sequences, including repeated flybys of the same body. Only Venus, Earth and Mars are considered for repeated flybys, since repeated flybys of the outer planets would result in TOFs exceeding 15 years. (Mercury is not considered for this study since its low mass and close proximity to the Sun make it a poor body for useful gravity assist.) In addition, once a flyby of an outer planet has occurred, only planets farther out from that body are considered for subsequent flybys. For example, once a flyby of Saturn has occurred, Uranus would be the only subsequent flyby body allowed before reaching Neptune.

Note that for this preliminary study, the method of finding all possible combinations of flyby bodies was only implemented for up to 3 flyby bodies (excluding Earth launch and Neptune arrival). For sequences of four flyby bodies, only paths from previous studies were considered. For example, all paths from the work by Petropoulos et al.[5] (for trajectories to Jupiter) were used in this paper, with the modification of adding Neptune as the final body after the Jupiter encounter. Paths of four flyby bodies from Spreen et al.[6] were also used, with the exchange of the final body Uranus for Neptune. In all, a total of 76 paths were investigated for this preliminary study.

Second, each path will be checked using a Tisserand graph, to determine whether the path is possible with regards to orbital energy. All paths deemed infeasible by the Tisserand graph are then eliminated from the list of possible candidates. This graphical method uses Tisserand's criterion, and was implemented by Strange and Longuski[13] in 2002. (An earlier version of this graphical method was developed by Labunsky et al. in 1998.[14]) The Tisserand graph has since been adapted by Johnson and Longuski in 2002 for aerogravity-assist trajectories,[15] by Chen et al. in 2008 for low-thrust gravity-assist trajectories,[16] and more recently by Campagnola and Russell in 2010 for gravity-assist trajectories that implement V_∞-leveraging maneuvers,[17] as well as for application to the circular-restricted three-body problem.[18]

Third, the satellite tour design program STOUR (developed by the Jet Propulsion Laboratory[19] and Purdue University[20,21]) is then used to solve the phasing problem, and determine which of the remaining candidate paths produce trajectories to Neptune within the launch period of 2020 to 2070. The program STOUR uses a patched-conic model with an analytic ephemeris to rapidly compute multiple gravity-assist trajectories. The program imposes a grid search of all candidate trajectories by stepping through specified launch dates and launch V_∞.

Fourth, from the list of candidate trajectories found from STOUR, the most desirable trajectories will be selected based on parameters such as launch V_∞, arrival V_∞, and TOF.

Note that throughout this paper, the problem of identifying candidate paths based on orbital energy (i.e. using the Tisserand graph), will be referred to as 'pathfinding.' The problem of identifying the remaining candidate paths as actual opportunities for the launch dates considered (i.e. using the patched-conic propagator STOUR), will be referred to as 'pathsolving.'

Selecting Candidate Paths: Pathfinding

The Tisserand graph is a plot of orbital specific energy versus radius of periapsis, and provides a graphical means of identifying potential paths. A detailed description of the theory behind this graphical method, and how it is developed using Tisserand's criterion, is provided by Strange and Longuski[13] and Labunsky et al.[14] In simple terms, the Tisserand graph can be described as follows: The lines on the Tisserand graph represent the locus of orbits with the same energy relative to a given planet. The intersection of lines of one planet with those of another indicates that there exist orbits about each planet with the same heliocentric energy. Thus, a transfer from one planet to another is possible from an energy standpoint (though the planet may not be in the correct location at the time the spacecraft crosses the planet's orbit). Knowledge of the planetary ephemerides and the solution of Lambert's problem are then required for pathsolving, in order to find out when in time the transfer orbit occurs.

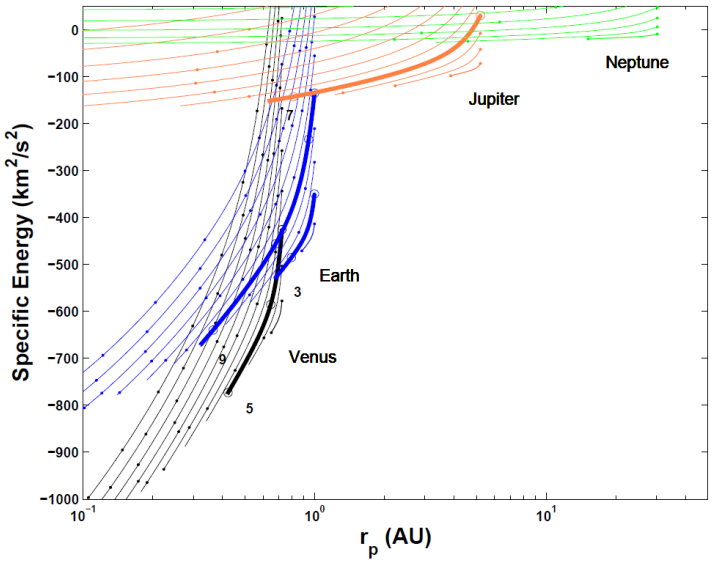

Figure 1. A Tisserand graph with the example path Venus-Earth-Earth-Jupiter-Neptune (VEEJN) indicated by the lines in bold.

To illustrate the use of the Tisserand graph, an example case is shown in Figure 1 for the path Venus-Earth-Earth-Jupiter-Neptune (VEEJN). The specific energy of the orbit is shown on the vertical axis and the radius of periapsis is shown on a logarithmic scale on the horizontal axis. In this example, lines are shown for Venus, Earth, Jupiter, and Neptune. The rightmost line for each planet represents a V_∞ of 1 km/s. V_∞ increases by 2 km/s with each line to the left (i.e. moving from right to left, the lines represent V_∞s of 1 km/s, 3 km/s, 5 km/s, etc.). The dots (or small circles if obstructed by a line in bold) along the V_∞ lines provide reference points for the amount of energy change that can be accomplished with a single flyby of the planet. This energy change is based on the maximum possible amount that the planet can rotate (or bend) the V_∞ vector. Note that the amount of bending possible is also based on the minimum flyby altitude, which in Figure 1 is uniformly set to 200 km.

A potential VEEJN path is highlighted by the bold lines in Figure 1. The path begins at Earth with 3 km/s as the chosen V_∞ of launch. By traversing this line down and to the left, an intersection with Venus is found at the line representing a V_∞ of 5 km/s. Following this line upward, several other V_∞ lines for Earth are encountered. The 9 km/s V_∞ line is of particular interest because it also intersects a Jupiter V_∞ line. The Earth V_∞ line for 9 km/s is then followed up and to the right (past the small circle), and on to an intersection with the Jupiter V_∞ line for 7 km/s. Passing the full distance between the two small circles on the Earth V_∞

line, indicates that the full amount of energy for a single Earth flyby has been achieved. Therefore, continuing beyond that point requires the use of the second Earth flyby. Finally, the Jupiter V_∞ line for 7 km/s is followed up and to the right until it intersects the Neptune V_∞ line for 3 km/s. The overall implication of this result is that a spacecraft with launch V_∞ of 3 km/s is capable of reaching Neptune by means of the flyby sequence Venus, Earth, Earth (again), Jupiter, and then arriving at Neptune with a V_∞ of 3 km/s.

Propagating in the Patched-Conic Model: Pathsolving

For this work, trajectories are propagated in the patched-conic model using STOUR, which is an automated low-fidelity tool for rapid trajectory design. By using the patched-conic model with analytic ephemeris, STOUR can quickly perform trajectory searches over large sweeps of launch dates and launch energies. STOUR can also compute trajectories with three different types of impulsive maneuvers: powered flyby,[22] broken plane or 'midcourse',[22] and V_∞-Leveraging.[23–25]

In practice, there are several constraints that limit the solution space, such as minimum flyby altitude for a given flyby body, maximum TOF for the entire trajectory to Neptune, and maximum launch energy. A summary of the constraints imposed on the trajectories considered for this broad search study are shown in Table 1.

Table 1. Trajectory Search Constraints

Parameter	Value
Minimum flyby altitude	300 km (Venus and Earth), 200 km (Mars), 100k km (Jupiter), 50k km (Saturn and Uranus)
Maximum TOF	15 yr
Maximum launch V_∞	20 km/s (Direct Launch), 17 km/s (1 flyby), 12 km/s (2 flybys), 9 km/s (3 flybys), 7 (4 flybys)
Maximum maneuver ΔV	3 km/s

For the case of minimum flyby altitude, drag losses must be avoided, as well as collisions with any rings (for the case of the outer planets). Since the outer planets can potentially provide a significant energy increase during a flyby, minimum altitudes were chosen just below the outer most (prominent) ring altitude to ensure that no trajectory opportunities are missed. The total TOF for each trajectory was limited to 15 years. This value is based on the lifetime of the Advanced Stirling Radioisotope Generator (ASRG), which is the power system recommended in the Neptune-Triton-KBO study for the decadal survey.[2] In the decadal survey, the ASRG is stated to provide a total mission lifetime of about 16 years. It is also stated that a one to two year mission lifetime at Neptune is recommended (for mission types that capture into the Neptune system). Thus, the total TOF for trajectories in this study were not allowed to exceed 15 years (for a one year mission) and ideally would not exceed 14 years (for a two year mission).

To determine the maximum allowed launch V_∞, many factors were considered. First and foremost, the goal in choosing these launch values is to encompass all foreseeable mission types to Neptune during the 2020 to 2070 time frame. Such mission types include both flyby and capture missions, as well as low and high payload mass missions (which will likely go hand in hand with the flyby and capture type missions, respectively). Additionally, the general purpose of using gravity assist bodies is to reduce the launch energy required to reach Neptune. Therefore, the maximum launch V_∞ considered can be reduced as more flyby bodies are added to the path. As an example of a single flyby body path, the New Horizons spacecraft trajectory (an earlier version of which is noted by Patel[22]) launched with a V_∞ of about 16 km/s, and then flew by Jupiter on its way to Pluto. Using New Horizons as a reference, a maximum launch V_∞ of 17 km/s was chosen for all paths to Neptune with only one flyby body, and 20 km/s was used for direct launch to Neptune. For two, three, and four flyby bodies, the maximum launch V_∞ values used by Landau et al.[8] were first considered for this study; however, for the case of three and four flyby bodies, some example simulations indicated that slightly larger launch V_∞ values provided a sizable increase in opportunities to Neptune. Thus,

for paths containing three or four flyby bodies, the maximum launch V_∞ values chosen are slightly larger than those used by Landau et al.

The patched-conic propagation tool is also capable if implementing impulsive maneuvers. For this paper, an algorithm designed by Patel[22] implements both "powered flyby maneuvers" (that are implemented 3 days after the flyby), and what Patel refers to as "midcourse maneuvers." In both cases, the required impulsive ΔV to reach the next body in the sequence is computed. The midcourse maneuver is applied approximately half way (with regards to TOF) along the transfer arc between the two bodies. This type of maneuver is sometimes referred to as a "broken-plane maneuver" and can be used to avoid transfer arcs that are significantly out of the orbit plane, when the transfer angle is near 180 degrees. Since this tool is designed for low-fidelity, rapid design, only a few flyby conditions are considered for this automated search. The details of this algorithm are discussed extensively by Patel.[22]

In this study, the Tisserand graph was also used to determine which paths would require a maneuver, as well as where in the path to place the maneuver to achieve the largest energy boost. Determining whether or not a maneuver was necessary for each path was done by attempting to reach Neptune on the Tisserand graph by starting from a launch V_∞ of 3 km/s. If reaching Neptune with this low value of launch V_∞ was feasible, then no maneuver was deemed necessary.

For many paths however, reaching Neptune on the Tisserand graph with 3 km/s of launch V_∞ was not feasible, and a maneuver had to be implemented. For these cases, a maneuver was represented on the Tisserand graph by shifting vertically upwards on the graph (representing an energy increase while holding perihelion constant). Determining how far upwards to shift on the Tisserand graph is based on the maximum allowed maneuver size. For this study, a maximum maneuver size of 3 km/s was used, which is consistent with the maneuver size chosen by Landau et al.[8] To shift upwards by 3 km/s on the Tisserand graph, one simply moves up until they reach the next constant V_∞ curve (to represent a maneuver size of 2 km/s), and then continues on upwards until reaching half way to the next V_∞ curve (to represent an additional 1 km/s boost in energy).

Representing maneuvers on the Tisserand graph allows one to estimate the best location in the path for a maneuver, which is done by identifying the maneuver location that gives the largest energy increase on the Tisserand Graph (i.e. is highest on the graph). For most cases, the 'best' maneuver location is after a flyby of the last inner planet in the path (before an outer planet is encountered). Intuitively, a maneuver will, in general, increase the V_∞ at the next flyby body and reduce the amount of bending that the flyby body can impose on the velocity vector. The effect of reduced bending capability is lessoned for the outer planets due to their large mass. Note that this method for determining the need and location of a maneuver is merely an energy based approximation to gage the effect of a maneuver. In addition, this method is really only applicable to a powered flyby maneuver, since the method involves adding to a value of V_∞ (which only has meaning with respect to a gravitational body).

A third type of maneuver is implemented for the special case of leveraging the V_∞ vector for a subsequent flyby of Earth after launch. Such a maneuver typically occurs at aphelion of a near resonant orbit—the true resonant orbit being referred to as the 'nominal' trajectory. The objective of this type of maneuver is to provide a relatively small burn at aphelion that results in a large increase in (and change in direction of) the V_∞ vector at the subsequent Earth encounter, which can then allow for a substantial gravity-assist at Earth. Such a leveraging maneuver is commonly referred to as a ΔV-EGA (for ΔV Earth gravity assist) or more generally, a V_∞-leveraging maneuver, where the leveraging body can be any body (as opposed to simply Earth). An extensive study of V_∞-leveraging maneuvers for multiple gravity-assist trajectories is discussed by Sims et al.[24,25]

V_∞-leveraging maneuvers were incorporated into the patched-conic propagator using a subroutine developed by A. J. Staugler.[23] This subroutine allows the user to specify launch date, nominal orbit, approximate deviation in launch V_∞ (from the nominal resonant orbit), location of the maneuver in terms of true anomaly, and number of heliocentric spacecraft and Earth revolutions between the maneuver and the Earth flyby. The subroutine can then compute (along with the patched-conic propagator) an automated search of V_∞-leveraging trajectories. For this preliminary study, only two paths were considered that used V_∞-leveraging, Earth-Neptune (EN) and Earth-Jupiter-Neptune (EJN), where the leveraging maneuver occurs at

aphelion before the Earth flyby. Note that the mention of Earth in these paths represents the Earth flyby and not Earth launch (which is not specified since Earth is the launch body for all paths considered in this paper). The nominal resonant orbits and deviation in velocity values were determined for the EN case from Sims,[25] and for the EJN case from Petropoulos et al.[5]

Launch and Capture ΔV

The ΔV corresponding to the launch V_∞ values used in the automated trajectory search can be computed if the hyperbolic periapsis is known. For this study, it is assumed that all trajectories launch from Earth from a 200 km circular low Earth orbit (LEO), giving a hyperbolic periapse radius of about 6578 km. For a given launch V_∞, the ΔV required to escape Earth from LEO can be determined from

$$\Delta V = \sqrt{V_\infty^2 + 2\mu/r_p} - \sqrt{\mu/r_p} \tag{1}$$

where r_p is the periapsis of the hyperbolic escape trajectory, and μ is the gravitational parameter for Earth.

For missions that capture into the Neptune system, the ΔV required for capture is given by

$$\Delta V = \sqrt{V_\infty^2 + 2\mu/r_p} - \sqrt{\mu(1+e)/r_p} \tag{2}$$

where μ is the gravitational parameter of Neptune, and e is the eccentricity of the capture orbit about Neptune. A minimum periapsis of 2.5 Neptune radii was recommended by the concept study in the Neptune-Triton-KBO decadal survey[2] and is used in this paper. With the periapsis radius known, the eccentricity of the capture orbit can be determined for a given capture orbit size (semimajor axis or orbital period). For this study, the ΔV corresponding to a given V_∞ was computed for various orbit sizes as shown in Figure 2.

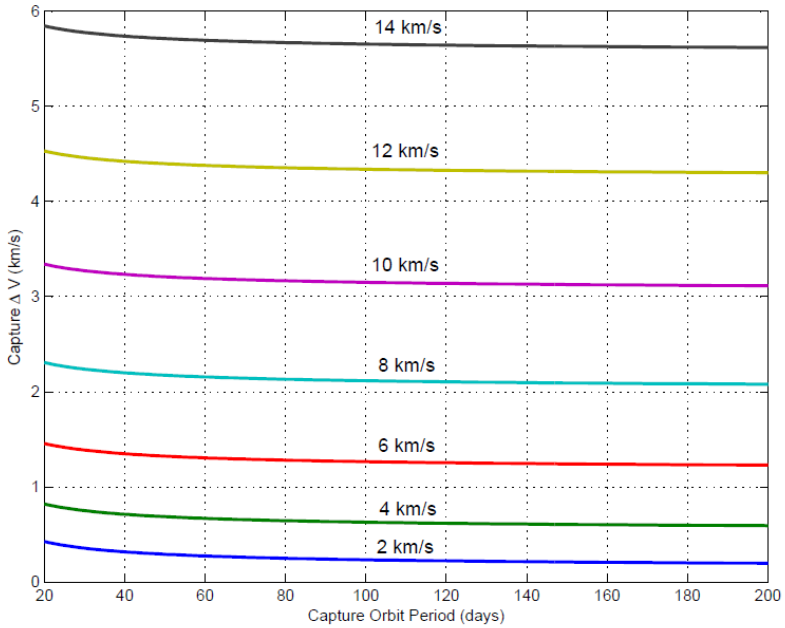

Figure 2. The curves on the plot above each represent a particular arrival V_∞ value, which is indicated by the annotation. Each curve appears to level out near an orbit size of 100 days.

Each curve shown in Figure 2 represents a particular arrival V_∞ at Neptune, as indicated by the annotations. The plot shows each curve approaching a horizontal asymptote as the orbit size increases. The minimum ΔV

values that the curves approach is the ΔV required for capture into a parabolic orbit—the limiting case. The plot shows that the ΔV is essentially at a minimum for all V_∞ curves once the orbit period exceeds about 100 days. An orbit of this size has a semimajor axis of about 95 Neptune radii, which is well below Neptune's sphere of influence (SOI) of about 3500 Neptune radii (where Neptune's gravity is dominant), and indicates that a capture orbit with a 100-day period is small enough to avoid significant solar gravity perturbations.

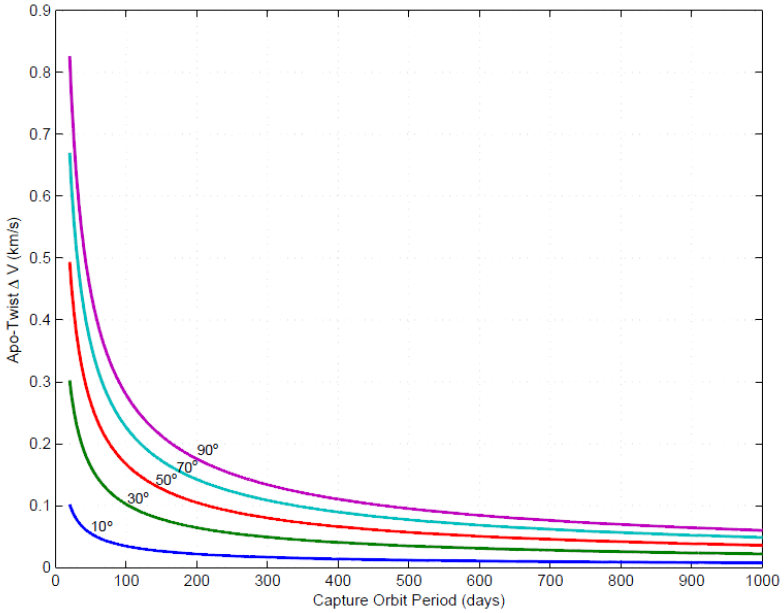

Figure 3. Apo-twist maneuver size for various required inclination changes at Neptune.

Another aspect of capture that can influence the choice of orbit size is the possible need for an inclination change. According to the Neptune-Triton-KBO study,[2] a capture mission will almost certainly require an inclination change—some requiring changes as large as 90^o. Such a change in inclination will likely require an additional ΔV maneuver, which can be minimized by applying the maneuver at apoapsis—referred to as an apo-twist maneuver. Figure 3 shows the required apo-twist ΔV for various capture orbit sizes. Each curve represents a required change in inclination from 10^o to 90^o. As expected, the curves show that larger orbit sizes require smaller maneuver sizes, and all level off at around a 1000-day orbit. This orbit size corresponds to a semimajor axis of about 440 Neptune radii, which is still well within Neptune's SOI.

Although many of the details for a particular mission to Neptune are uncertain, Figures 2 and 3 indicate that any capture orbit at Neptune will likely have at least a 100-day orbital period to keep the capture maneuver size low and, if applied, the apo-twist maneuver size low as well. Since an orbit size of 100 days is a bit more conservative for determining the ΔV required for capture, a 100-day orbit was assumed to compute all capture ΔV values, in this paper.

RESULTS

Of the total 76 paths investigated for this preliminary study, only 21 produced trajectories between the launch dates 2020 and 2070. The complete list of paths that provided trajectories is given in the following list, where each flyby body is represented by the first letter in the planet name (i.e. V for Venus, E for Earth, M for Mars, etc.) and are listed in the order of encounter. Note that the values in parentheses indicate a resonant orbit between consecutive flybys of the same planet. For example, (3:1) represents a 3 to 1 resonant orbit with 3 target body revolutions (about the Sun) and 1 spacecraft revolution (about the Sun). Also note that the " * " indicates that a maneuver is performed between the two bodies in the sequence. The paths that produces trajectories are as follows:

N, M⋆N, JN, SN, ME⋆N, M⋆JN, JSN, VVV⋆N (2:1, 5:1), VVE⋆N (2:1), VV⋆JN, VV⋆JN (2:1), VV⋆JN (3:1), VEE⋆N, VEE⋆N (3:1), VEE⋆N (4:1), VE⋆JN, ME⋆JN, VVV⋆JN, VVV⋆JN (1:1, 2:1), VVV⋆JN (2:1, 2:1), VVV⋆JN (2:1, 3:1), VVV⋆JN (2:1, 4:1), VVV⋆JN (2:1, 5:1), VVE⋆JN, VVE⋆JN (2:1), VEEJN, VEEJN (2:1), VEEJN (3:1), VEEJN (4:1), VEE⋆SN, VEE⋆SN (3:1), VEE⋆SN (4:1), VEM⋆JN, MEE⋆JN, MEE⋆JN (2:1), MEE⋆JN (3:1), MEE⋆JN (4:1), and ⋆EJN.

The path ⋆EJN uses a V_∞-leveraging maneuver, where the '⋆' in this case indicates that the maneuver (performed at aphelion) occurs before the Earth flyby. The use of a V_∞-leveraging maneuver for this path was found to produce trajectories using the nominal resonances (3:1), (4:1), and (5:1).

Of the paths that found trajectories listed above, several found as little as one to four total trajectories over the entire search space. For all of these cases, the resulting trajectories required large maneuver ΔVs and large launch and arrival V_∞ values, and where not considered further in this study. The trajectories that were eliminated as candidates are: ME⋆N, VVV⋆N (2:1, 5:1), and VEM⋆JN.

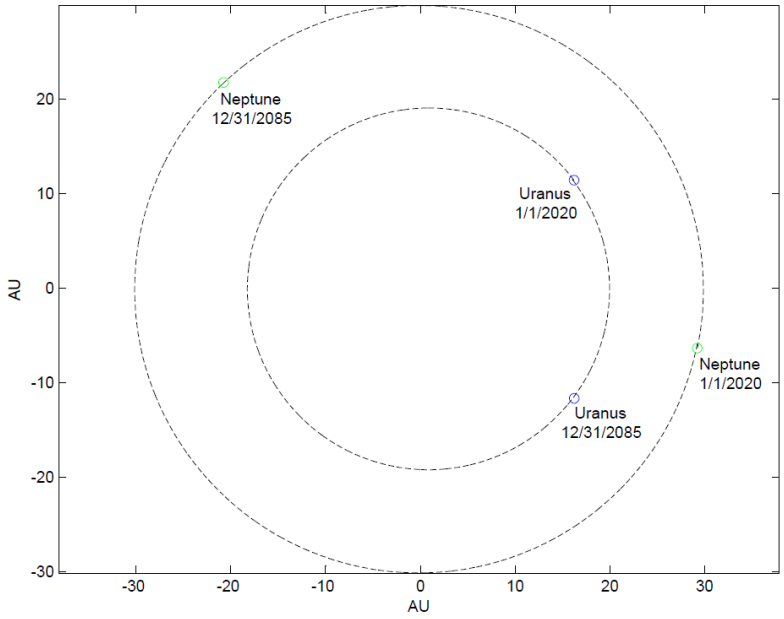

Figure 4. The relative positions of Uranus (inner orbit) and Neptune (outer orbit) on 1/1/2020 and 12/31/2070 illustrates that a large bending angle is required to find trajectories that include consecutive Uranus and Neptune encounters.

It is also important to note that no trajectories were found that flyby Uranus, due to the poor relative position of Uranus with respect to Neptune for the years 2020 through 2085 (2070+15 year TOF). The locations of Uranus and Neptune on 1/1/2020 and 12/31/2085 are shown in Figure 4, where it is clear that (for orbital motion in a counterclockwise direction), an encounter with Neptune after a flyby of Uranus requires a large bending angle of nearly 170^o to 180^o for both relative positions shown (and every orientation in between for this time span). To further verify that trajectories with paths containing consecutive Uranus-Neptune encounters are infeasible, the path UN was propagated (in the patched-conic model) with a minimum flyby altitude at Uranus of only 300 km, and found no trajectories.

To determine which trajectories in each path are the most desirable, many factors are considered. In general, the pathsolving process results in a set of candidate trajectories that occur within the search period, but differ in many parameters, including: launch date, launch V_∞, arrival V_∞, and time of flight. For this paper, trajectories that minimize the required arrival ΔV are favored over those that minimize the time of flight, and any trajectories with a time of flight less than 14 years are considered to be equally acceptable.

The components of the total mission ΔV are determined by the launch V_∞, the maneuver ΔV, and the arrival V_∞. Neptune capture missions levy more constraining requirements on arrival V_∞ than do Neptune flyby missions. Therefore for this selection process of best case candidates, capture missions were exclusively considered.

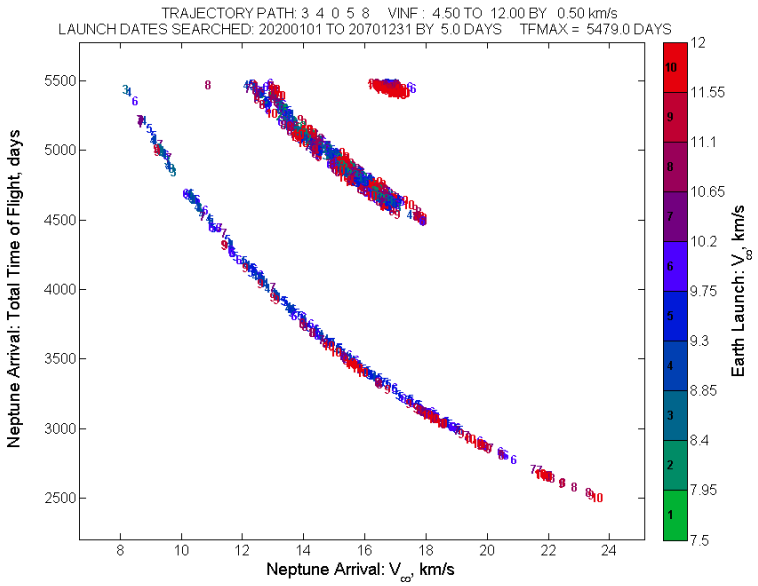

Figure 5. Plot of candidate path solutions for M⋆JN.

The first step in selecting the best (or very nearly the best) trajectory in a set of solutions is to plot the total time of flight against the Neptune arrival V_∞. Figure 5 is an example of such a plot for the path M⋆JN, in which the indices (and color) indicate the launch V_∞ (specified by the key to the right of the plot). We focus on the upper-left-hand corner of the plot, which includes trajectories with low arrival V_∞, and TOF around 14 to 15 years (about 5110 to 5480 days). In fact, the figure shows a general trend of trajectories that trade TOF and arrival V_∞, where it is shown that for longer times of flight lower arrival V_∞ trajectories are found, and vise versa. Thus, the top left region is likely to contain the best case trajectory for the path with regards to arrival V_∞ and TOF (since only a TOF of 14 years is needed).

Table 2. Best Candidates for the Path M⋆JN.

Trajectory	Arrival V_∞ (km/s)	Maneuver ΔV (km/s)	Launch V_∞ (km/s)	TOF (yr)	Launch Date
1	8.22	1.13	8.50	14.88	02/17/2031
2	8.32	2.22	9.00	14.83	01/23/2031
3	8.52	2.19	10.00	14.66	12/29/2030
4	8.69	0.04	10.50	14.28	03/14/2031
5	8.69	1.57	10.50	14.28	03/14/2031
6	8.73	0.02	10.50	14.23	03/14/2031
7	8.74	1.50	10.50	14.22	03/14/2031
8	8.83	0.87	9.00	14.27	01/18/2031
9	8.99	2.93	9.50	14.12	01/13/2031
10	9.10	1.62	9.00	13.88	02/27/2031

While investigating the upper left portion of plots such as that shown in Figure 5, two important details to assess are the size of the launch V_∞ and the maneuver ΔV (if a maneuver exists). Since the maneuver size is not visible from this plot shown, the trajectories in this region must be looked at in more detail to find the best one for the path. For example, Table 2 summarizes the ten leftmost trajectories from Fig. 5. Trajectory number 1 has the lowest arrival V_∞ and the lowest launch V_∞ as well as a relatively small maneuver ΔV, and was therefore selected as the best (or at least very nearly the best) case for the path M⋆JN. A similar analysis was performed for each path that produced trajectories.

Table 3. Best Case Trajectories for Each Path.

Path	Launch Date	$V_{\infty,L}$ (km/s)	ΔV_L (km/s)	$V_{\infty,A}$ (km/s)	ΔV_A (km/s)	TOF (yr)	Maneuver ΔV (km/s)	Total ΔV (km/s)
N	8/22/2067	12.50	8.87	7.91	2.07	13.70	–	10.95
M⋆N	5/2/2035	14.50	10.42	8.16	2.19	13.43	0.21 (PF)	12.82
JN	3/23/2032	10.00	7.09	8.70	2.46	13.46	–	9.54
SN	4/20/2022	12.00	8.50	8.71	2.46	12.96	–	10.96
M⋆JN	2/7/2031	8.50	6.12	9.37	2.81	13.67	0.02 (PF)	8.95
JSN	6/20/2058	11.00	7.78	8.31	2.26	13.41	–	10.04
VVE⋆N (2:1)	1/31/2020	8.00	5.82	11.31	3.91	14.55	2.89 (PF)	12.62
VV⋆JN	8/1/2029	7.50	5.54	10.95	3.70	13.88	2.98 (PF)	12.21
VV⋆JN (2:1)	9/11/2066	7.00	5.26	11.02	3.74	14.80	1.50 (PF)	10.50
VEE⋆N	3/21/2060	4.50	4.11	11.03	3.75	14.94	2.77 (PF)	10.63
VEE⋆N (3:1)	6/17/2068	8.50	6.12	10.80	3.61	14.96	2.85 (PF)	12.58
VE⋆JN	9/20/2029	4.50	4.11	10.21	3.27	14.30	2.23 (PF)	9.60
ME⋆JN	7/8/2067	6.50	5.00	10.56	3.47	14.41	1.20 (Mid)	9.67
VVV⋆JN	7/12/2028	6.50	5.00	11.62	4.10	14.60	2.15 (PF)	11.25
VVV⋆JN (2:1, 5:1)	8/1/2028	6.00	4.75	12.08	4.39	14.73	1.97 (PF)	11.11
VVE⋆JN	7/29/2042	6.50	5.00	9.66	2.96	14.73	0.41 (PF)	8.37
VVE⋆JN (2:1)	1/24/2028	7.00	5.26	11.94	4.30	14.90	–	9.56
VEEJN	7/13/2026	4.00	3.93	14.27	5.84	14.79	–	9.77
VEEJN (2:1)	11/3/2053	5.00	4.31	11.65	4.12	14.69	–	8.43
VEE⋆SN	10/29/2053	4.00	3.93	11.76	4.19	14.91	2.562 (PF)	10.68
VEE⋆SN (3:1)	5/17/2053	4.00	3.93	12.36	4.57	14.97	2.939 (PF)	11.43
MEE⋆JN	4/19/2065	6.50	5.00	13.29	5.17	14.76	2.749 (PF)	12.92
MEE⋆JN (2:1)	5/4/2065	6.50	5.00	13.19	5.11	14.78	0.693 (PF)	10.80
⋆EJN (3:1)	3/23/2053	7.24	5.39	11.96	4.32	14.85	1.48 (Lev)	11.19
⋆EJN (4:1)	5/2/2053	8.19	5.94	12.50	4.65	14.65	1.03 (Lev)	11.62
⋆EJN (5:1)	4/18/2028	8.81	6.32	12.72	4.80	14.69	1.38 (Lev)	12.50

Table 3 summarizes the results of the process described above, and shows the best case trajectory for each of the various paths examined. Note that the type of maneuver performed (if applicable) is indicated in the parenthetical to the right of the maneuver size, where 'PF' represents a powered flyby, 'Mid' a midcourse maneuver, and 'Lev' a V_∞-Leveraging maneuver. Additionally, the subscripts 'L' and 'A' indicate conditions at launch and arrival, respectively.

Of the trajectories listed in Table 3, several paths stand out, and it may be of interest to see the available launch date opportunities throughout the 2020 to 2070 time span for these paths. From the work of Landau et al[8] as well as from the Neptune-Triton-KBO study,[2] there seems to be a trend to keep the total ΔV size after launch to remain at around 3 km/s or below. Therefore, all paths that were capable of producing trajectories with total maneuver and capture ΔV around 3 km/s or below were investigated further with regards to launch date. These paths include: N, M⋆J, JN, SN, M⋆JN, and JSN. Because this list is relatively short, the constraint was relaxed to include all paths with total maneuver and capture ΔV below 5 km/s, which adds to the list of paths: ME⋆JN, VVE⋆JN, VVE⋆JN (2:1), and VEEJN (4:1). In addition, a lower launch V_∞ in practice allows for a larger payload mass, and can in turn allow more propellant to be stored for maneuver and capture ΔVs. (For the case of missions that merely fly by the Neptune system, no capture ΔV is required at all). Therefore, paths that provided a total ΔV of less than 10 km/s were also investigated with regard to launch date opportunities—adding to the list of paths: VE⋆JN and VEEJN. As a final consideration, because paths that do not include JGAs are of interest for launch dates when Jupiter is not available, any path with a total ΔV of less than 11 km/s, and that did not include a JGA, was also considered for further investigation with regards to launch date. This final adjustment adds VEE⋆N and VEE⋆SN to the total list of paths.

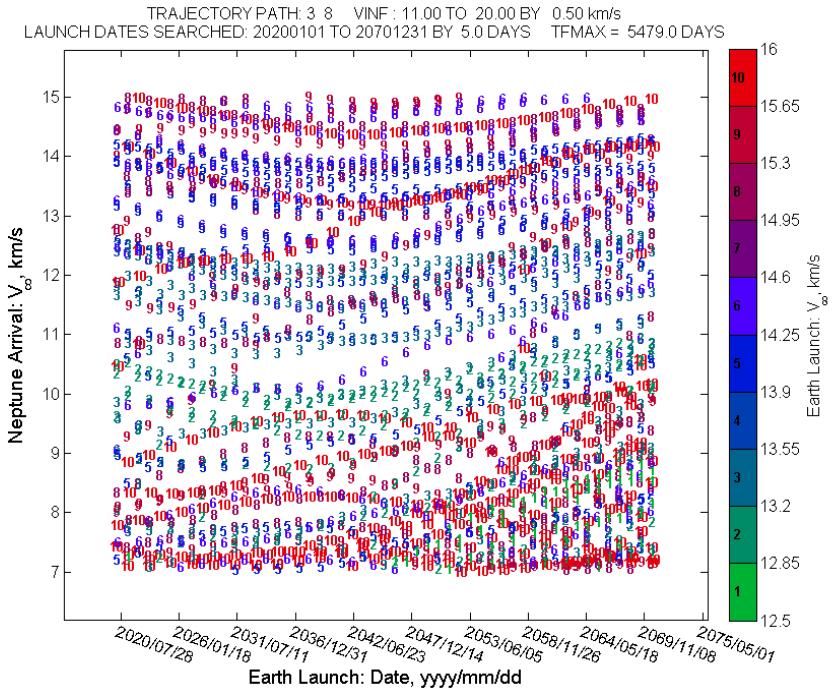

Figure 6. N (direct launch) trajectories.

Figures 6 through 19 show all launch opportunities for the previously mentioned paths of interest. Of the total 14 paths considered, only 5 do not include flybys of Jupiter. These are N (direct launch), M⋆N, SN, VEE⋆N and VEE⋆SN. For the case of direct launch to Neptune, the maximum launch V_∞ shown (in Figure 6) was reduced to allow for the more desirable cases to be clearly visible. In each figure, note that each index number (and color) represents a particular launch V_∞, which is specified by the key to the right of each plot.

It is important to keep in mind, when looking at Figures 6 through 19 , the behavioral trends observed in this study regarding TOF and arrival V_∞. For all opportunities discussed in this investigation, the TOF is less than 15 years; however, the opportunities with shorter TOFs will tend to exist where the arrival V_∞ is low, and the opportunities with longer TOFs will tend to exist where the arrival V_∞ is high. A representative case that exhibits this behavior was shown previously in Figure 5 for the path M⋆JN.

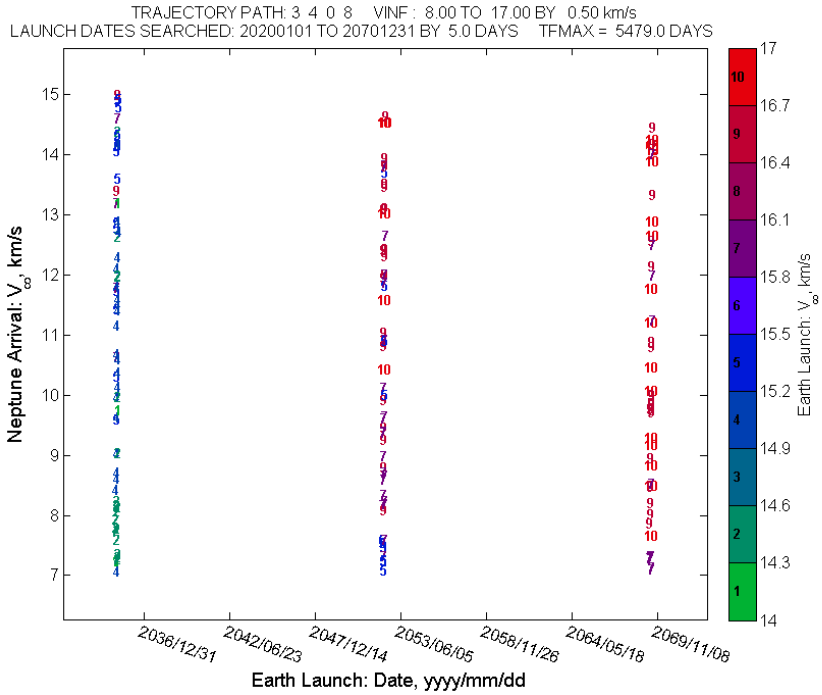

Figure 7. M*N trajectories.

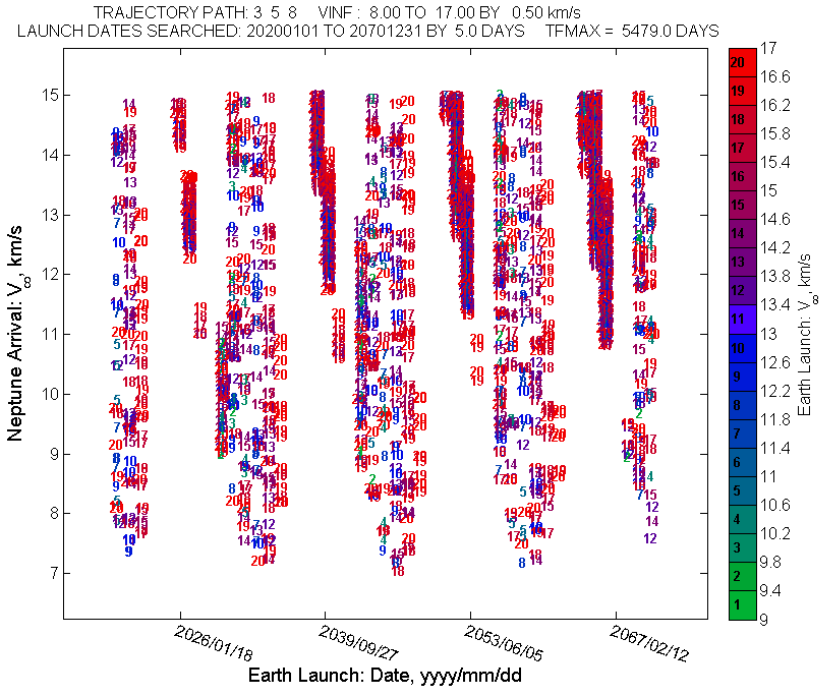

Figure 8. JN trajectories.

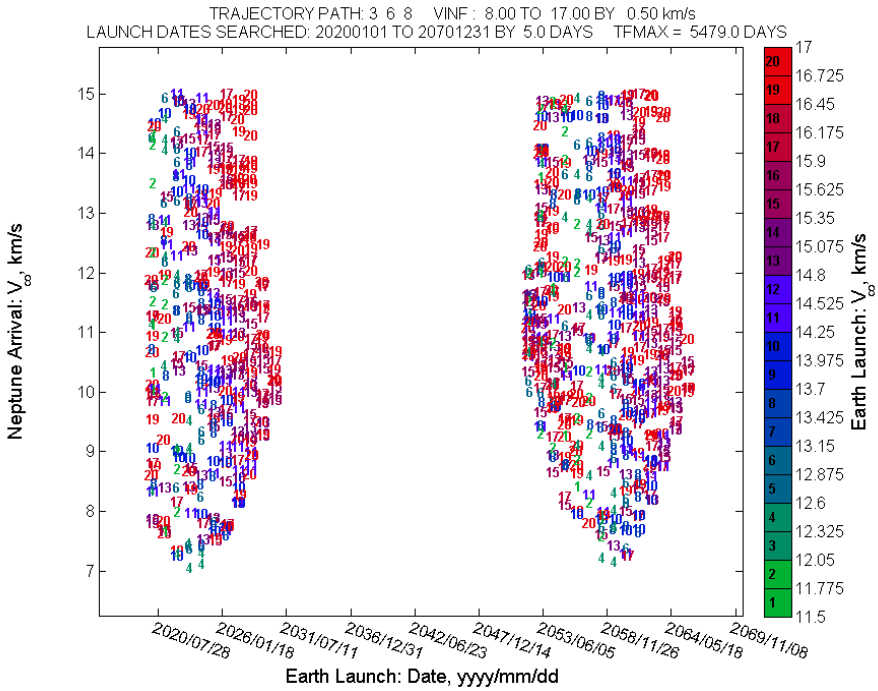

Figure 9. SN trajectories.

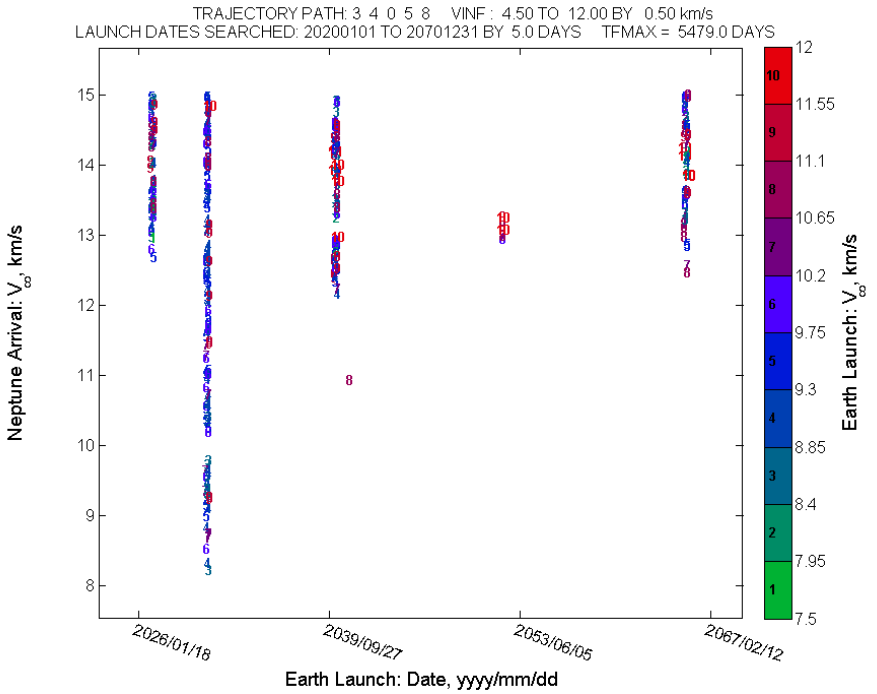

Figure 10. M*JN trajectories.

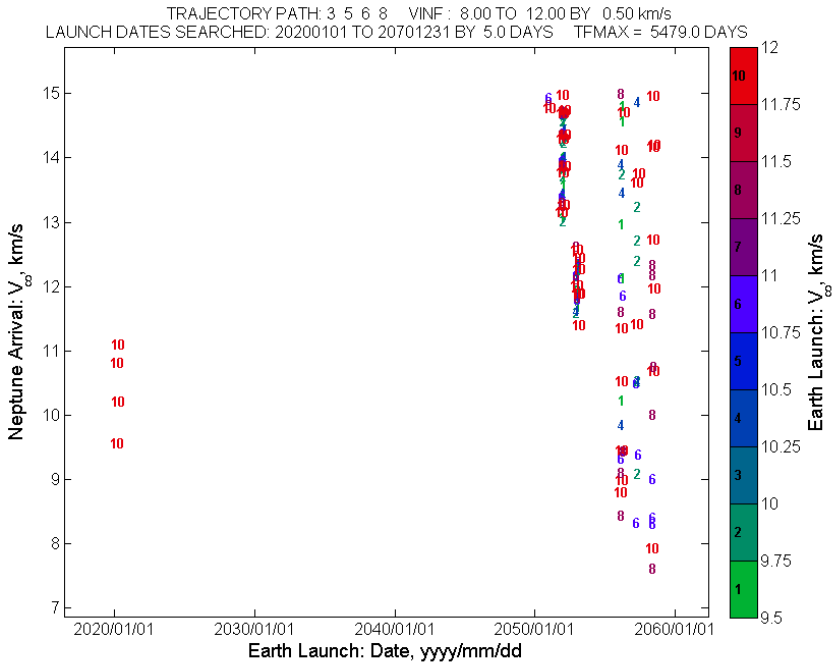

Figure 11. JSN trajectories.

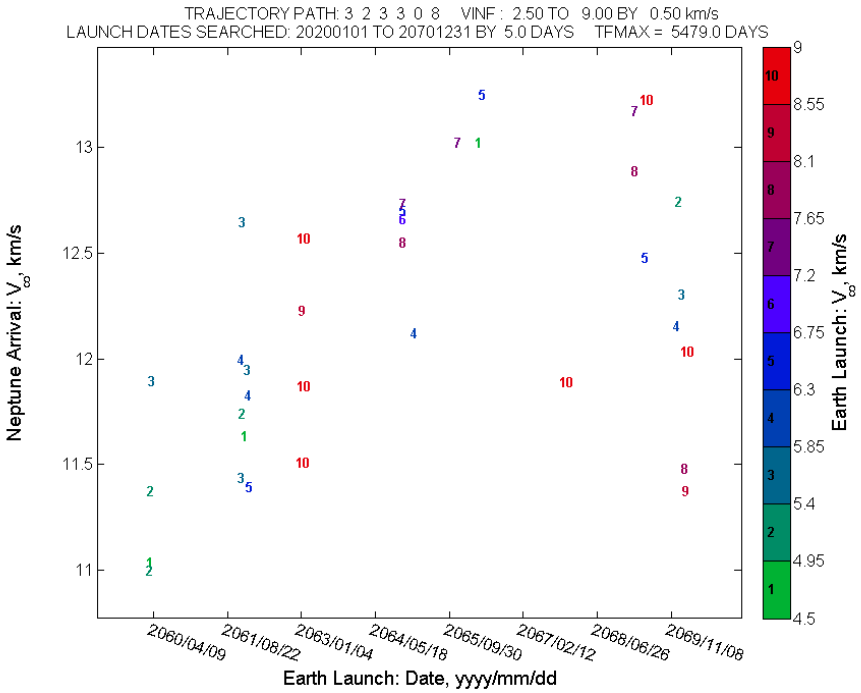

Figure 12. VEE*N trajectories.

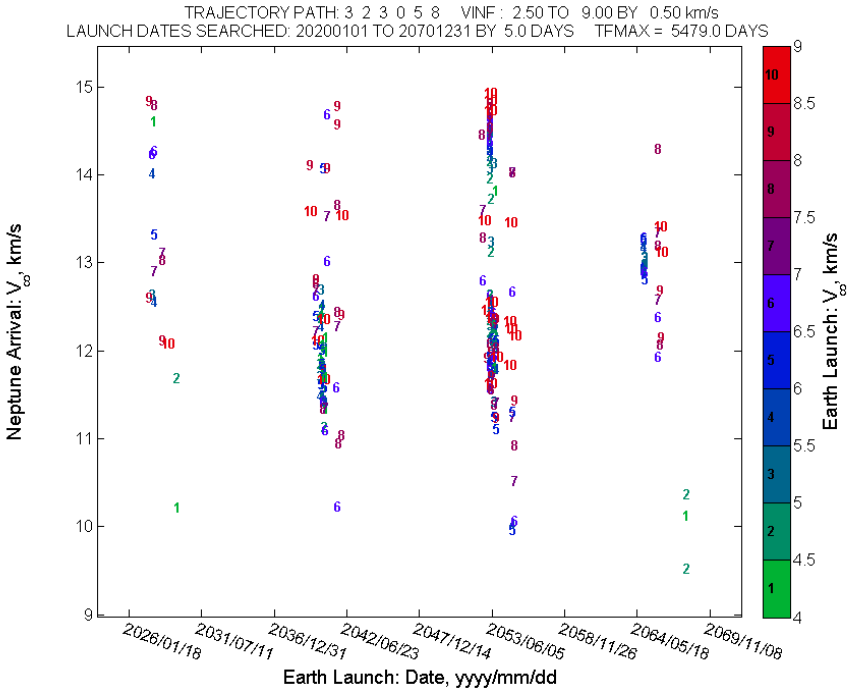

Figure 13. VE*JN trajectories.

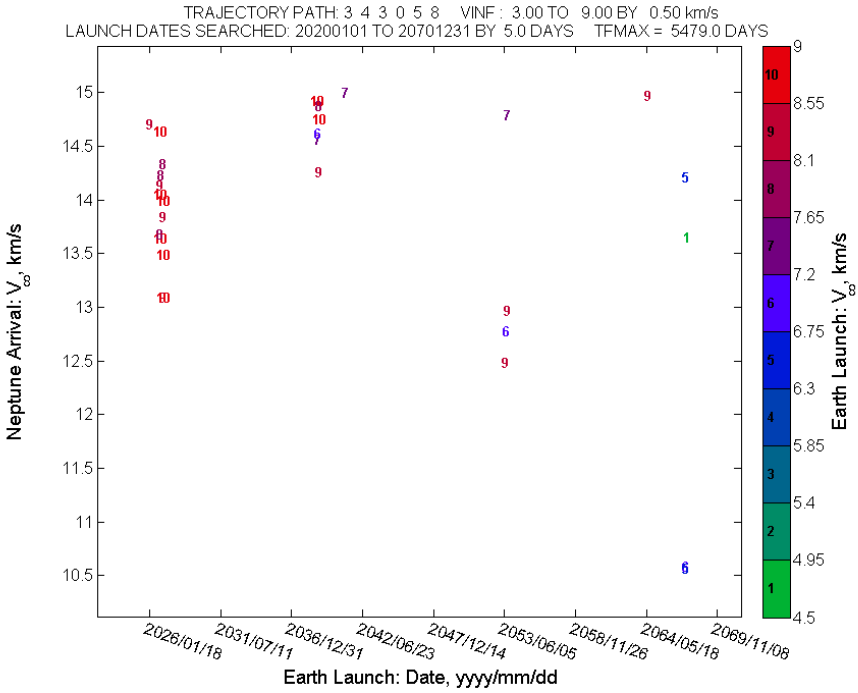

Figure 14. ME*JN trajectories.

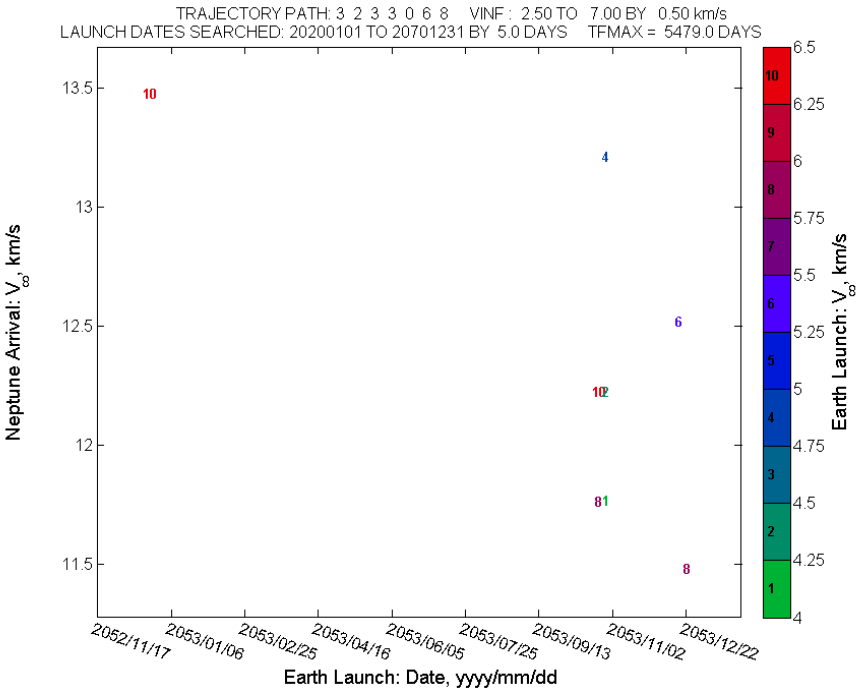

Figure 15. VEE*SN trajectories.

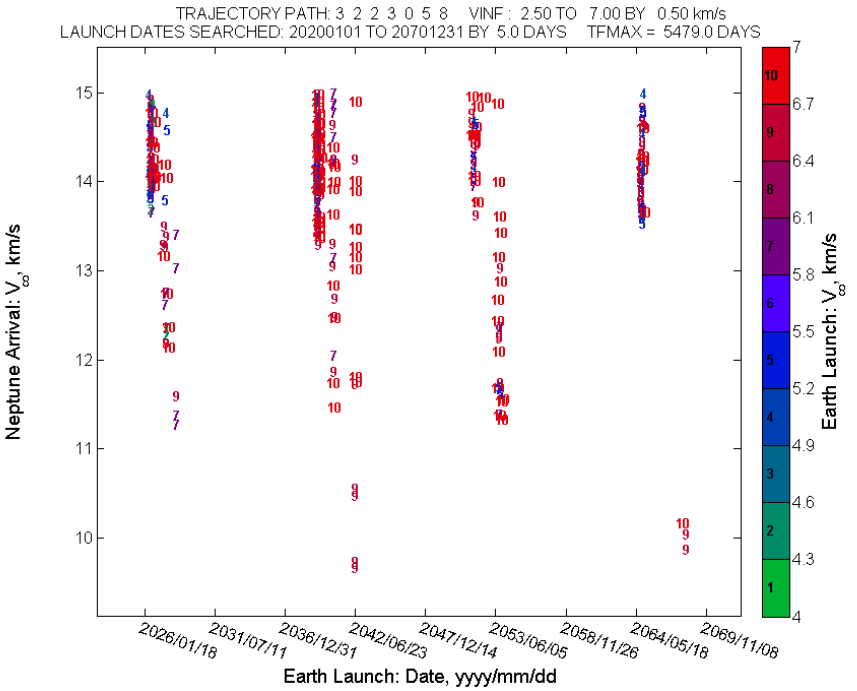

Figure 16. VVE*JN trajectories.

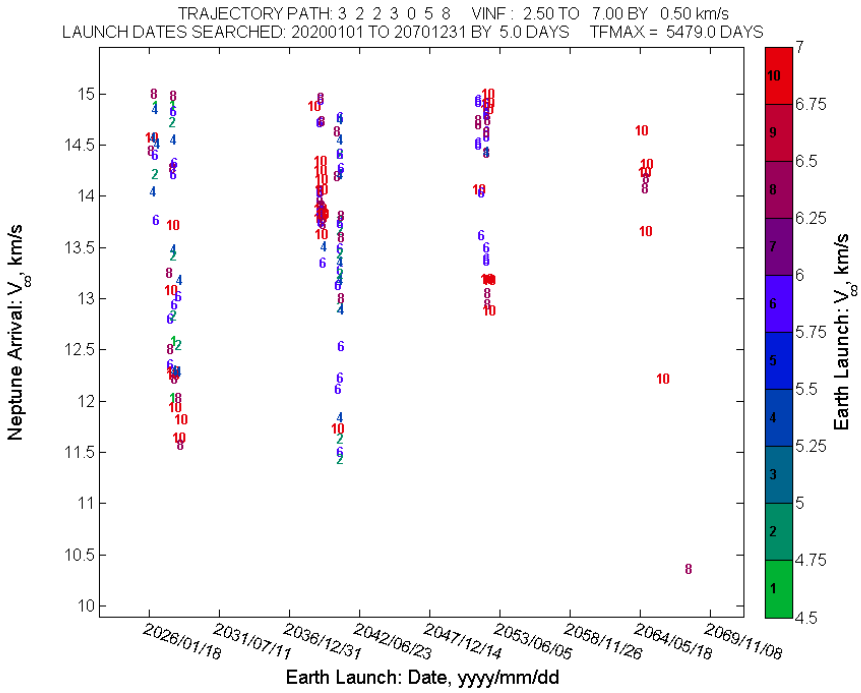

Figure 17. VVE*JN (2:1) trajectories.

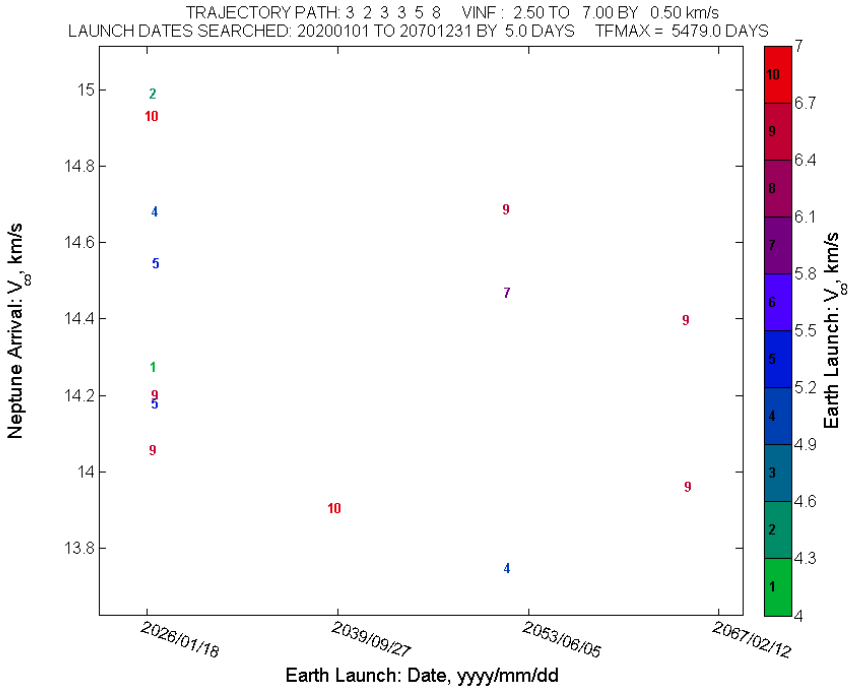

Figure 18. VEEJN trajectories.

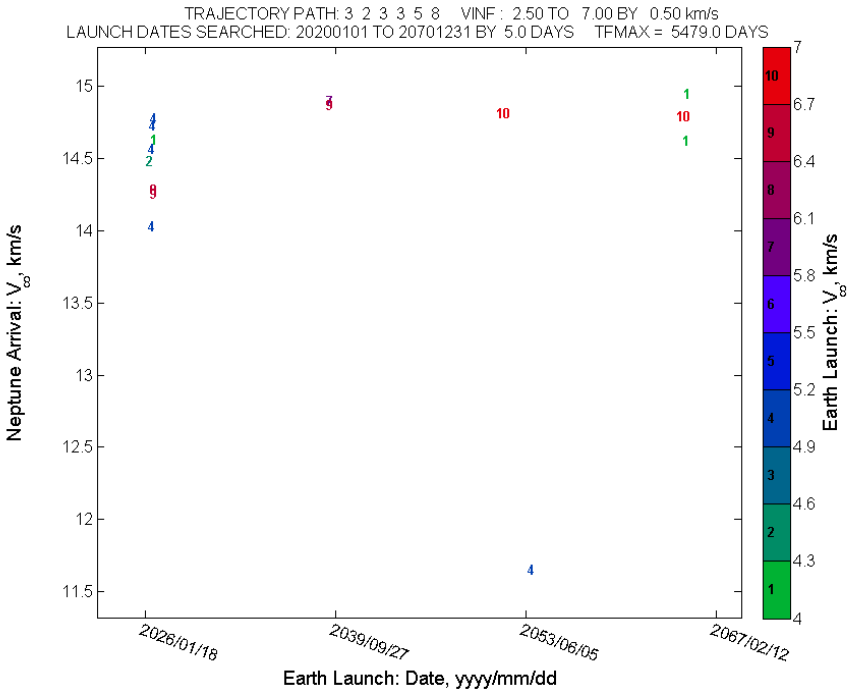

Figure 19. VEEJN (2:1), (3:1), and (4:1) trajectories.

Of the paths that do not use a JGA, the two that have by far the most opportunities are the direct launch and the path SN, shown in Figures 6 and 9. In the near future, the results from the path JN in Figure 8 show that (to obtain an arrival V_∞ below 10 km/s), there is a gap from around 2022 to 2030 where Jupiter is not available. Conveniently, 2022 to 2030 is a range of times when Saturn is available (as shown in Figure 9 for the path SN), but likely at the cost of a higher launch V_∞. One issue with the SN opportunities is that they do not provide any benefit over the direct launch to Neptune, which has nearly a continuous range of launch opportunities throughout the 2020 to 2070 time frame, and is capable of providing a smaller total ΔV cost (as shown in Table 3).

Note that although the discussion of this section has focused primarily on missions that capture into the Neptune system, opportunities of potential interest for flyby missions can be found in Figures 6 through 19. Although there is no capture ΔV required for a flyby mission, the arrival V_∞ value may still be of concern. To gage what maximum arrival V_∞ values are acceptable, the value for the example flyby trajectory in the Neptune-Triton-KBO study[2] of about 14 km/s was used as a reference, and values of up to 15 km/s were ultimately used for Figures 6 through 19.

Of the favorable paths discussed in this study, many contain three flyby bodies or less, which may seem counterintuitive since more flybys allow for lower launch V_∞. The trouble is that adding more flyby bodies also increases the energy of the transfer orbit to Neptune, and therefore increases the arrival V_∞, and corresponding capture ΔV. For capture missions to Neptune, the goal then is to provide just enough energy to reach Neptune (within the 15 year time limit), so that upon arrival, the spacecraft is traveling relatively slow to match the slow velocity of Neptune itself.

Another aspect of these trajectories, is that flybys of the inner planets constrain perihelion to be at least as low as the inner planets themselves—that is until a flyby of one of the outer planets occurs. Thus, for paths that do not include outer planet flybys, to reach Neptune with low perihelion, a highly eccentric orbit must exist with aphelion at least as far out as Neptune. The trouble therein is that a spacecraft with just enough energy to reach Neptune will be moving very slowly as it approaches Neptune (near aphelion of the

spacecraft's trajectory). This type of trajectory is good for keeping the arrival V_∞ small, but will likely not reach Neptune within the 15 year TOF constraint. On the other hand, for higher energy orbits (and therefore higher aphelia), Neptune could be reached within a 15 year TOF, but would arrive with a larger arrival V_∞. This general trade of orbit energy with TOF gives some insight into the behavior seen in the results of this study, where long TOFs seem to correspond with low arrival V_∞ and short TOFs with high arrival V_∞.

CONCLUSION

In this paper, ballistic trajectories to Neptune (with at most one impulsive maneuver) were investigated for launch dates ranging from 2020 to 2070. Of the 76 paths investigated, only 21 produced trajectories that satisfied the constraints. Most of these paths required a flyby of Jupiter, which also provided the opportunities with the lowest required launch and arrival ΔVs. For launch dates when Jupiter is not available as a gravity-assist body (such as from about 2022 to 2030), direct launch or flybys of Saturn can be used, but both require a higher ΔV at launch in most cases. Additionally, due to the relative heliocentric positions of Uranus and Neptune (during the time periods considered in this study), all trajectories with consecutive encounters of Uranus and Neptune were found to be infeasible.

A cursory investigation of the use of V_∞-leveraging maneuvers (with Earth as the leveraging body) did not produce attractive trajectories compared to other favorable paths (such as those shown in Figures 6 – 19). For all paths that found trajectories, opportunities to Neptune exhibited a behavioral trend that exchanged TOF for arrival ΔV.

It is hoped that the preliminary gravity-assist and ΔV gravity-assist trajectories presented here will provide mission designers and planetary scientists with a wide variety of potential options over the next 50 years for the exploration of the most distant planet in the Solar System.

ACKNOWLEDGMENTS

We thank Dave L. Skinner for generously sharing his skills and his time. Without his computational support, this research would not have been possible. We also thank Nathan J. Strange for his guidance and his advice. We had many useful conversations with him concerning missions to the Ice Giants, and we are very appreciative of his help.

REFERENCES

[1] Hubbard, W.B., "Ice Giants Decadal Study," Planetary Science Decadal Survey: Mission Concept Study Final Report, National Aeronautics and Space Administration, June 2010.

[2] Marley, M.S. and Dudzinski, L.A., "Neptune-Triton-KBO Study Final Report," Planetary Science Decadal Survey and JPL Rapid Mission Architecture: Mission Concept Study Final Report, National Aeronautics and Space Administration, Feb. 2010.

[3] Longuski, J.M. and Williams, S.N., "The Last Grand Tour Opportunity to Pluto," *The Journal of the Astronautical Sciences*, Vol. 39, No. 3, July – Sep. 1991, pp. 359 – 365.

[4] Sims, J.A., Staugler, A.J., and Longuski, J.M., "Trajectory Options to Pluto via Gravity Assists from Venus, Mars, and Jupiter," *Journal of Spacecraft and Rockets*, Vol. 34, No. 3, May – June 1997, pp. 347 – 353.

[5] Petropoulos, A.E., Longuski, J.M., and Bonfiglio, E.P., "Trajectories to Jupiter via Gravity Assists from Venus, Earth, and Mars," *Journal of Spacecraft and Rockets*, Vol. 37, No. 6 Nov. – Dec. 2000.

[6] Spreen, C.M., Mueterthies, M.J., Kloster, K.W., and Longuski, J.M., "Preliminary Analysis of Ballistic Trajectories to Uranus Using Gravity-Assists from Venus, Earth, Mars, Jupiter, and Saturn," AAS Paper No. 11-623, AAS/AIAA Astrodynamics Specialist Conference, Girdwood, AK, July 31 – Aug. 4, 2011.

[7] Melman, J., Orlando, G., Safipour, E., Mooij, E., and Noomen, R., "Trajectory Optimization for a Mission to Neptune and Triton," AIAA Paper No. 2008-7366, AIAA/AAS Astrodynamics Specialist Conference, Honolulu, HI, Aug. 18 – 21, 2008.

[8] Landau, D., Lam, T., and Strange, N., "Broad Search and Optimization of Solar Electric Propulsion Trajectories to Uranus and Neptune," *Advances in the Astronomical Sciences*, Vol. 135, Part 3, No. AAS 09-428, 2009, pp. 2093 – 2112.

[9] Sims, J.A., Finlayson, P.A., Rinderle, E.A., Vavrina, M.A., and Kowalkowski, T.D., "Implementation of a Low-Thrust Trajectory Optimization Algorithm for Preliminary Design," AIAA Paper No. 2006-6746, AIAA/AAS Astrodynamics Specialist Conference, Keystone, CO, Aug. 21 – 24, 2006.

[10] Casalino, L., Colasurdo, G., and Pastrone, D., "Optimal Low-Thrust Escape Trajectories Using Gravity Assist," *Journal of Guidance, Control, and Dynamics*, Vol. 22, No. 5, Sep. – Oct. 1999.

[11] Zimmer, S. and Ocampo, C., "Use of Analytical Gradients to Calculate Optimal Gravity-Assist Trajectories," *Journal of Guidance, Control and Dynamics*, Vol. 28, No. 2, March – April 2005.

[12] Yam, C.H., Di Lorenzo, D., and Izzo, D., "Constrained Global Optimization of Low-Thrust Interplanetary Trajectories," IEEE Congress on Evolutionary Computation, Barcelona, Spain, July 18 – 23, 2010.

[13] Strange, N.J. and Longuski, J.M., "Graphical Methods for Gravity-Assist Trajectory Design," *Journal of Spacecraft and Rockets*, Vol. 39, No. 1, Jan. – Feb. 2002.

[14] Labunsky, A., Papkov, O., and Sukhanov, K., "Multiple Gravity Assist Interplanetary Trajectories," Earth Space Institute Book Series, Gordon and Breach, London, 1998, pp. 33 – 68.

[15] Johnson, W.R. and Longuski, J.M., "Design of Aerogravity-Assist Trajectories," *Journal of Spacecraft and Rockets*, Vol. 39, No. 1, Jan. – Feb. 2002.

[16] Chen, K.J., Kloster, K.W., and Longuski, J.M., "A Graphical Method for Preliminary Design of Low-Thrust Gravity-Assist Trajectories," AIAA Paper No. 2008-6952, AIAA/AAS Astrodynamics Specialist Conference, Honolulu, HI, Aug. 18 – 21, 2008.

[17] Campagnola, S. and Russell, R.P., "Endgame Problem Part 1: V_∞-Leveraging Technique and the Leveraging Graph," *Journal of Guidance, Control, and Dynamics*, Vol. 33, No. 2, March – April 2010.

[18] Campagnola, S. and Russell, R.P., "Endgame Problem Part 2: Multibody Technique and the Tisserand-Poincaré Graph," *Journal of Guidance, Control, and Dynamics*, Vol. 33, No. 2, March – April 2010.

[19] Rinderle, E.A., "Galileo Users Guide, Mission Design System, Satellite Tour Analysis and Design Subsystem," Jet Propulsion Laboratory, Report JPL D-263, California Institute of Technology, Pasadena, CA, July 1986.

[20] Williams, S.N., "Automated Design of Multiple Encounter Gravity-Assist Trajectories," M.S. Thesis, School of Aeronautics and Astronautics, Purdue University, West Lafayette, IN, Aug. 1990.

[21] Longuski, J.M. and Williams, S.N., "Automated Design of Gravity-Assist Trajectories to Mars and the Outer Planets," *Celestial Mechanics and Dynamical Astronomy*, Vol. 52, Aug. 1991, pp. 207 – 220.

[22] Patel, M.R., "Automated Design of Delta-V Gravity-Assist Trajectories for Solar System Exploration," M.S. Thesis, School of Aeronautics and Astronautics, Purdue University, West Lafayette, IN, Aug. 1990.

[23] Staugler, A.J., "STOUR (Satellite Tour Design Program) User's Guide for the ΔV-EGA and V_∞-Leveraging Routines," School of Aeronautics and Astronautics, Purdue University, West Lafayette, IN, June 1996.

[24] Sims, J.A., Longuski, J.M., and Staugler, A.J., "V_∞ Leveraging for Interplanetary Missions: Multiple-Revolution Orbit Techniques," *Journal of Guidance, Control, and Dynamics*, Vol. 20, No. 3, 1997, pp. 409 – 415.

[25] Sims, J.A., "Delta-V Gravity-Assist Trajectory Design: Theory and Practice," PhD Thesis, School of Aeronautics and Astronautics, Purdue University, West Lafayette, IN, 1996.